Sylvester, Z., Durkin, P.R., Hubbard, S.M., and Mohrig, D., 2021, Autogenic translation and counter point bar deposition in meandering rivers: GSA Bulletin, https://doi.org/10.1130/B35829.1.

Supplemental Material

Figure S1. (A) Boxplots of Mamoré River channel widths for the 31 Landsat scenes used in the study. The boxes represent the first, second, and third quartiles; the ends of the whiskers represent one and a half times the interquartile range. Dashed line is the median channel width (350.0 m) for all measurements; this is the value that was used to calculate the bar type index. (B) Boxplots of measured migration rates for the 30 time steps. The boxes represent the first, second, and third quartiles; the ends of the whiskers represent one and a half times the interquartile range. Dashed line represents 60.0 m/year, the value used to normalize migration rates in the bar type index calculation.

Figure S2. (A) Map of a segment of the Mamoré River in 1999. Yellow polygons show the locations of bar accretion between 1998 and 1999; blue centerline corresponds to 1998, and red centerline to 1999. Numbered zero-migration locations are shown as black dots and are the same as in (B). Arrows mark the counter-point bars. (B) Measured dimensionless curvatures, migration rates, and bar type indices along a segment of the Mamoré River (same as in (A)).

List of animations

1. Time-lapse evolution of area 1. Mapped BTI values on left, uninterpreted false-color image on the right.
2. Time-lapse evolution of combined area 2 and 3 with mapped BTI values shown.
3. Time-lapse evolution of area 2. Mapped BTI values on left, uninterpreted false-color image on the right.
4. Time-lapse evolution of area 3. Mapped BTI values on left, uninterpreted false-color image on the right.

The banks and the centerlines of the Mamore River have been mapped in 31 Landsat 4, Landsat 5 and Landsat 8 scenes, spanning the years between 1986 and 2018. The following is a list of the product identifiers for these Landsat scenes:

LT05_L1TP_232070_19860716_20170217_01_T1
LT05_L1TP_232070_19870703_20170212_01_T1
LT05_L1TP_232070_19880806_20170207_01_T1
LT05_L1TP_232070_19890708_20170202_01_T1
LT05_L1TP_232070_19900727_20170129_01_T1
LT05_L1TP_232070_19910612_20170126_01_T1
LT04_L1TP_232070_19920724_20170122_01_T1
LT05_L1TP_232070_19930719_20170118_01_T1
LT05_L1TP_232070_19940807_20170112_01_T1
LT05_L1TP_232070_19950810_20170107_01_T1
LT05_L1TP_232070_19960609_20170104_01_T1

LT05_L1TP_232070_19970714_20161230_01_T1
LT05_L1TP_232070_19980717_20161223_01_T1
LT05_L1TP_232070_19990720_20161217_01_T1
LT05_L1TP_232070_20000706_20161214_01_T1
LT05_L1TP_232070_20010725_20161210_01_T1
LT05_L1TP_232070_20030715_20161205_01_T1
LT05_L1TP_232070_20040701_20161130_01_T1
LT05_L1TP_232070_20050704_20161126_01_T1
LT05_L1TP_232070_20060723_20161120_01_T1
LT05_L1TP_232070_20070811_20161111_01_T1
LT05_L1TP_232070_20080712_20161030_01_T1
LT05_L1TP_232070_20090731_20161022_01_T1
LT05_L1TP_232070_20100702_20161014_01_T1
LT05_L1TP_232070_20110806_20161009_01_T1
LC08_L1TP_232070_20130710_20170504_01_T1
LC08_L1TP_232070_20140713_20170421_01_T1
LC08_L1TP_232070_20150801_20170406_01_T1
LC08_L1TP_232070_20160718_20170323_01_T1
LC08_L1TP_232070_20170721_20170728_01_T1
LC08_L1TP_232070_20180622_20180623_01_RT

No scenes were used for 2002 and 2012, as none of the available images had the quality needed for the analysis.

Figure S1a shows the distribution of channel widths for each Landsat scene. Widths were measured at every 25 m along the channel, using an approach that relies on the 'shapely' Python package. The observed width variability is largely due to the variations in river stage; this width variability also has an influence on migration rate measurements. Migration rates are overestimated for time steps when there is a significant decrease in river stage; and underestimated for time steps when there is a relatively large increase in river stage (Fig. S1b). However, having scenes for almost every year was more important than the drawbacks of the variability due to stage variations, as this approach allowed us to map in detail the channel migration even in locations with very large migration rates. These locations often coincide with counter-point bars, the main focus of this study.

With the exception of time steps when the river stage increased significantly (marked with arrows in Fig. S1a), measured migration rates tend to mimic the along-channel curvature, with a downstream phase lag (Fig. S2).

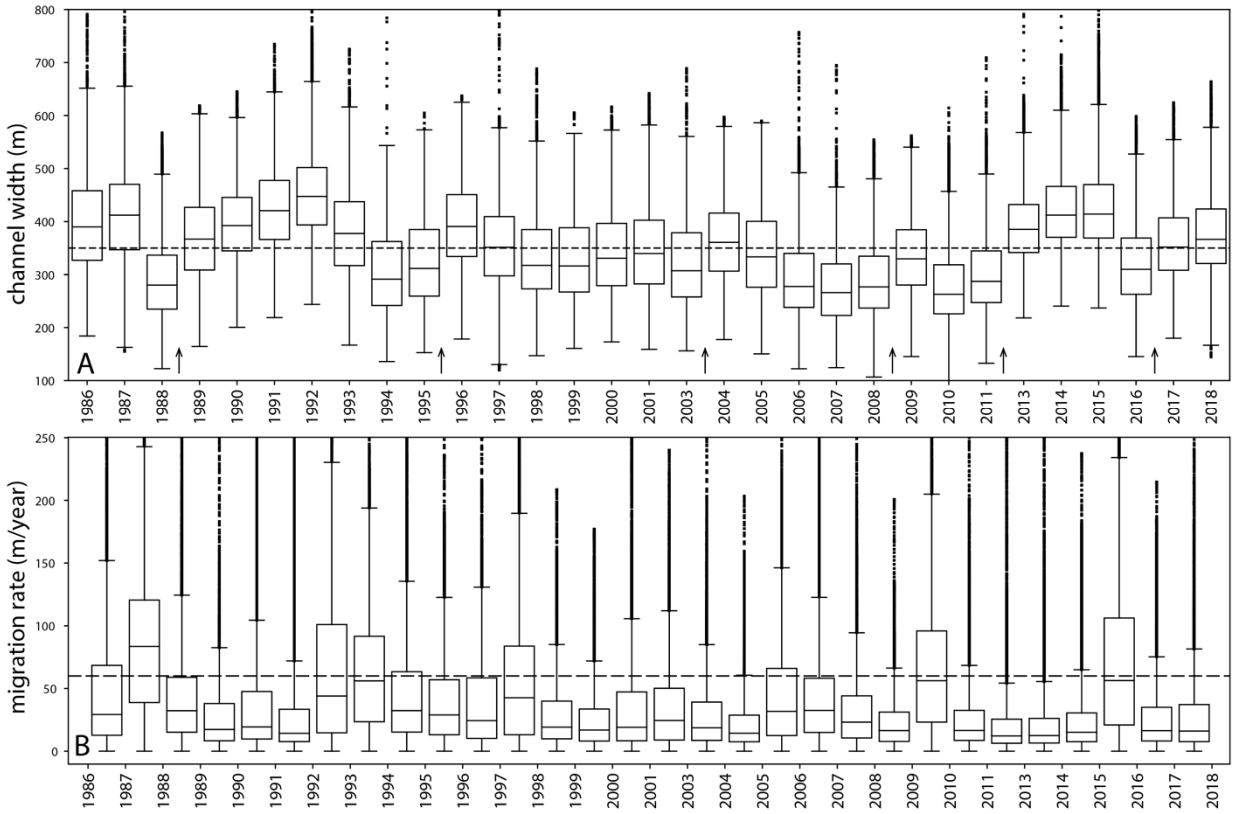

Figure S1. (A) Boxplots of Mamoré River channel widths for the 31 Landsat scenes used in the study. The boxes represent the first, second, and third quartiles; the ends of the whiskers represent one and a half times the interquartile range. Dashed line is the median channel width (350.0 m) for all measurements; this is the value that was used to calculate the bar type index. (B) Boxplots of measured migration rates for the 30 time steps. The boxes represent the first, second, and third quartiles; the ends of the whiskers represent one and a half times the interquartile range. Dashed line represents 60.0 m/year, the value used to normalize migration rates in the bar type index calculation.

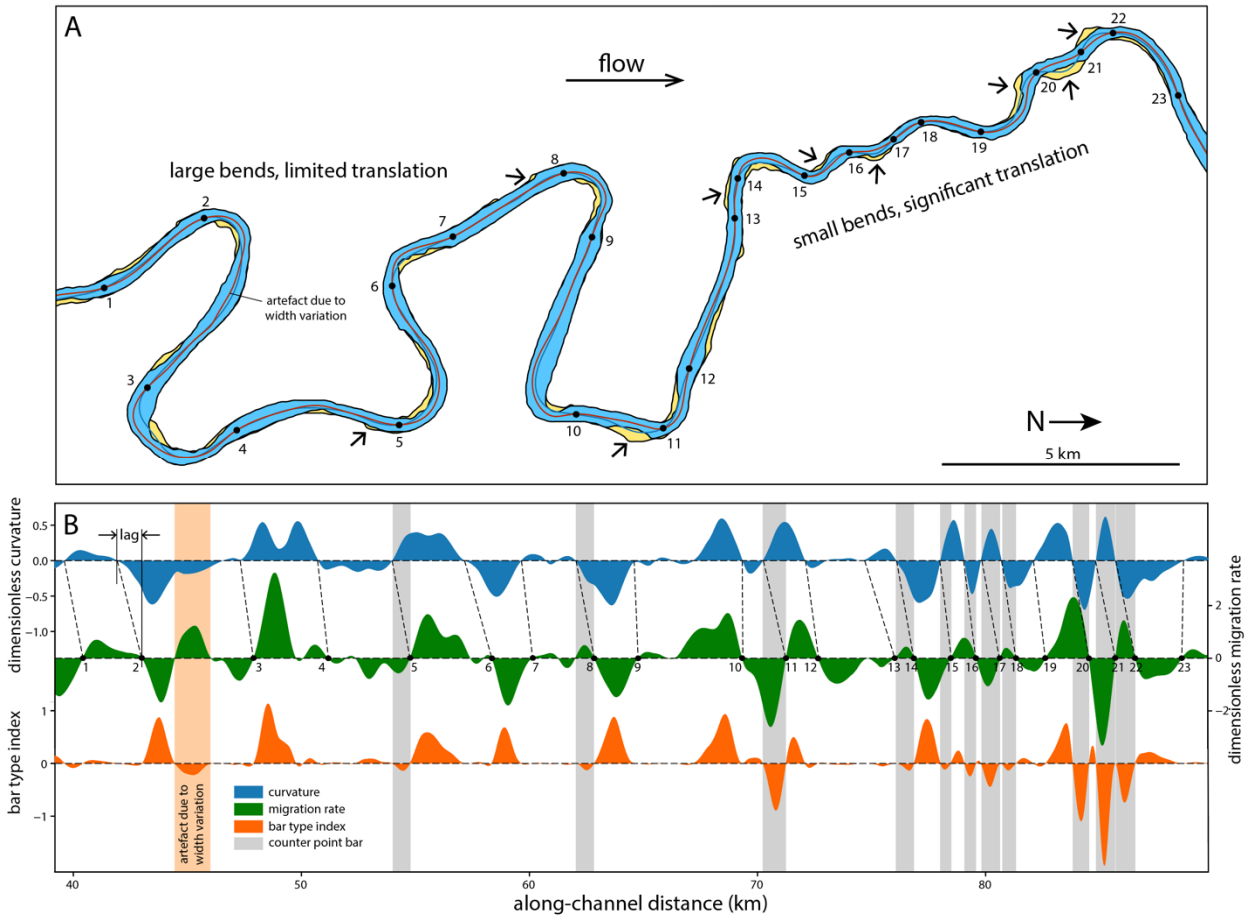

Figure S2. (A) Map of a segment of the Mamoré River in 1999. Yellow polygons show the locations of bar accretion between 1998 and 1999; blue centerline corresponds to 1998, and red centerline to 1999. Numbered zero-migration locations are shown as black dots and are the same as in (B). Arrows mark the counter-point bars. (B) Measured dimensionless curvatures, migration rates, and bar type indices along a segment of the Mamoré River (same as in (A)).